

ABSOLUTE INSTABILITY OF A DOUBLE RING JET – NUMERICAL STUDY

JAROSŁAW BIJAK
ANDRZEJ BOGUSŁAWSKI

Czestochowa University of Technology, Institute of Thermal Machinery, Poland
e-mail: abogus@imc.pcz.czyst.pl; jbijak@imc.pcz.czyst.pl

The paper is aimed at analyzing the influence of external flow on absolutely unstable modes of a ring jet with recirculation zone. The double ring jet is also considered. The investigation is carried out by means of the linearized, inviscid spatio-temporal stability theory. Calculations are based on the shooting method for asymmetric azimuthal mode. During the numerical experiment, absolutely unstable modes were identified. No major influence of the external stream on the stability of the flow was also proved.

Key words: absolute instability, double jet, shooting method

1. Introduction

The linear spatio-temporal theory is applied in order to show the most unstable modes of axisymmetric jets and to analyze the influence of an external co-flow on the convective and absolute instabilities. The applied spatio-temporal analysis follows the formulation of Briggs (1964) and Bers (1983) for plasma physics. The complex wave number and the complex frequency are used in the perturbation equation. Using this approach, an absolutely unstable flow can be defined as the one which has a mode with zero group velocity in the upper half of the complex frequency plane. If the zero group velocity lies in the lower half plane, the flow is called convectively unstable. In the field of fluid mechanics, the concept was comprehensively described by Huerre and Monkewitz (1990).

The analysis is based mainly on the numerical work of Michalke (1999) concerning a single ring jet with recirculation zone. Michalke has proved, on the basis of the inviscid linearized theory, that the flow is only convectively unstable for the axisymmetric mode and becomes absolutely unstable for the

first azimuthal mode with back flow greater than -0.3 of the maximum axial velocity. It seems to be interesting to analyze whether an additional outer ring jet stabilizes or destabilizes the flow and what is the effect of the second recirculation zone between both co-axial jets.

The starting point in the research is the configuration considered by Michalke, i.e. a single jet with recirculation zone. The known solution of the flow is used to speed up the saddle point searching for further slightly modified configurations. The iterative procedure is applied, i.e. solution of one configuration serves as an estimation for the next one. The base flow is first modified by increasing the outer co-flow up to 0.9 of the maximum velocity. The changes are sufficiently small to keep the solution close to the previous one. Next, the second recirculation zone is created by decreasing velocity in the region between the jets to the level of -0.3 of the maximum velocity. The final velocity profile is the double annular jet.

Contents of the paper is as follows: Section 2 contains a short introduction to absolute/convective instability concepts, in Sections 3 and 4 the scope of the work and numerical procedure are described, results are in Section 5, the paper is summarized in the last Section 6.

2. Spatio-temporal stability analysis

The classical linearized stability analysis involves a mean parallel flow and an infinitesimal perturbation superimposed on it. The fluctuations are decomposed into elementary instability waves

$$\hat{p}(r) \exp[i(\alpha x - \omega t)] \quad (2.1)$$

of complex wave number α and complex frequency ω ; in the spatial stability theory the frequency is real whilst the wave number is complex, similarly the temporal theory considers complex frequency and real wave number. The x variable is the spatial coordinate in flow direction, r is the radial direction and t is time. The $\hat{p}(r)$ is an amplitude which satisfies the Orr-Sommerfeld equation. In these circumstances the differential equation leads to eigenvalue and the eigenfunction problem, where ω/α is the eigenvalue and $\hat{p}(r)$ the eigenfunction. Next, according to the stability theory, the flow is stable if the Green function of the differential equation is zero along all rays $x/t = \text{const}$

$$\lim_{t \rightarrow \infty} G(x, t) = 0 \quad \text{for all} \quad \frac{x}{t} = \text{const} \quad (2.2)$$

and the flow is unstable if the Green function along at least one ray $x/t = \text{const}$ is infinite

$$\lim_{t \rightarrow \infty} G(x, t) = \infty \quad \text{for at least one} \quad \frac{x}{t} = \text{const} \quad (2.3)$$

Contrary to the predecessors, the spatio-temporal theory distinguishes two types of instability: convective and absolute. The first one means that initial perturbation is amplified and convected away from its origin. In the second type, the perturbation spreads in all directions and eventually contaminates all spatial positions. It follows that the unstable flow is convectively unstable if

$$\lim_{t \rightarrow \infty} G(x, t) = 0 \quad \text{for} \quad \frac{x}{t} = 0 \quad (2.4)$$

and is absolutely unstable if

$$\lim_{t \rightarrow \infty} G(x, t) = \infty \quad \text{for} \quad \frac{x}{t} = 0 \quad (2.5)$$

The above condition for absolutely unstable flow is necessary but not sufficient. The additional constraint was formulated in plasma physics and is often referred to Briggs (1964) or Fainberg *et al.* (1961) condition. It states that the absolutely unstable flow has a saddle point in the space (α, ω) and the point is formed by coalescence of an upstream and a downstream α branches – it is also called a pinching requirement. To find such a saddle point, a map of $\alpha(\omega)$ is constructed where the α branch coalescence can be easily identified. Additionally, as it was shown by Chomaz *et al.* (1988), a flow is absolutely unstable if the saddle point lies within the region

$$0 < \text{Im}(\omega) \leq \text{Im}(\omega(\alpha_m)) \quad (2.6)$$

The α_m is the wave number of the most amplified wave in time.

Exhaustive description of the spatio-temporal theory can be found in the papers of Bers (1983) or Huerre and Monkewitz (1990).

3. Scope of the work

The starting point of the numerical experiment is the Michalke velocity profile Michalke (1999)

$$\begin{aligned} U(r) &= 4BF(r)[1 - BF(r)] \\ F(r) &= \frac{1}{1 + [\exp(ar^2) - 1]^N} \\ B &= \frac{1}{2}(1 + \sqrt{1 - U_0}) \end{aligned} \quad (3.1)$$

With the parameters $U_0 = -0.3$, $N = 1$, the profile represents a ring jet with a back flow on the jet axis. The maximum jet velocity defines the radius of the jet R , so that $U_{max} = U(R)$. The nondimensional Michalke profile – normalized by length R and velocity U_{max} – is shown in Figure 1. The nondimensional form will be used in the calculation. For convenience, the introduced notation is preserved and further in the text all symbols are treated as nondimensional.

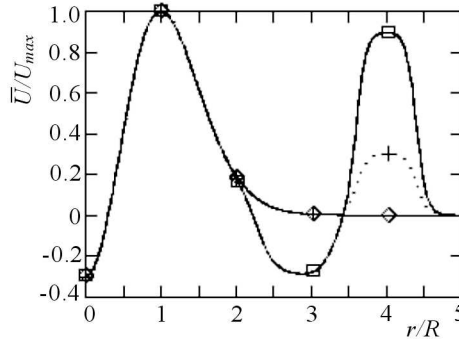


Fig. 1. Velocity profiles: for the base, Michalke profile \diamond , flow with small external co-flow (0.3) $+$ and final profile with co-flow (0.9) and back-flow (-0.3) \square

For the velocity shape mentioned above, Michalke had found one saddle point which satisfied the pinching requirement. The influence of an external co-flow and secondary back flow on the saddle point locus will be investigated. The modification of the base profile is done by addition of an outer velocity profile of the form Michalke and Hermann (1982)

$$U_{outer} = \frac{U_2}{2} - \frac{U_2}{2} \tanh\left[\left(|r - R_2| - R_{2w}\right)\frac{\theta}{2}\right] \quad (3.2)$$

The profile has a single ring jet shape with the velocity magnitude U_2 . R_2 is the distance of the ring from the axis, R_{2w} is the width of the ring and θ controls the mixing layer thickness. The profile is superimposed on the base one (proposed by Michalke (1982)) in order to keep the Michalke profile unaffected. Superposition of two velocity profiles created by the above equation with positive and negative U_2 and with the base profile, leads to the final co-axial flow with two recirculation zones – one on the axis and the second one between two inflow streams. During the numerical experiment the velocity magnitude U_2 varied from 0.1 to 0.9, in the case of co-flow, and from 0 to -0.3 for the back-flow. The recirculation zone is taken into account only for flows with co-flow greater than 0.3. The remaining parameters of the external flow are summarized in Table 1. The flows with and without recirculation zone are shown in Figure 1.

Table 1. Parameters of the external flow

	U_2	R_2	R_{2w}	θ
co-flow	0.1 to 0.9	4	0.4	15
back flow	0 to -0.3	2.8	0.5	10

4. Numerical procedure

The inviscid, linear stability equation (Boguslawski, 2002; Jendoubi and Strykowski, 1994)

$$\frac{d^2\hat{p}(r)}{dr^2} + \left(\frac{1}{r} - \frac{2}{U-c} \frac{dU}{dr}\right) \frac{d\hat{p}(r)}{dr} - \left(\alpha^2 + \frac{m^2}{r^2}\right) \hat{p}(r) = 0 \tag{4.1}$$

where: $c = \omega/\alpha$ – the complex phase velocity, has an asymptotic solution in the area of zero velocity gradient dU/dr of the form

$$\hat{p}(r) = C_1 I_m(\alpha r) + C_2 K_m(\alpha r) \tag{4.2}$$

where: C_1, C_2 – arbitrary constants; I_m, K_m – modified Bessel functions of order m .

The second order differential equation (??) can be transformed to the first order using the substitution

$$\chi = -i\alpha \frac{\hat{p}}{\hat{v}} \tag{4.3}$$

and

$$\frac{d\hat{p}(r)}{dr} = -i\alpha(U-c)\hat{v} \tag{4.4}$$

The resulting relation

$$\frac{d\chi}{dr} = -\alpha^2(U-c) + \chi \left[\frac{1}{U-c} \left(\frac{\alpha^2 + \left(\frac{m}{r}\right)^2}{\alpha^2} \chi - \frac{dU}{dr} \right) + \frac{1}{r} \right] \tag{4.5}$$

is solved numerically.

The boundary conditions for the above equation is derived from equation (4.2) and the presented substitution. The equations (4.3) and (4.4) lead to the relation for χ

$$\chi = -\alpha^2(U-c) \frac{\hat{p}}{\frac{d\hat{p}(r)}{dr}} \tag{4.6}$$

At the boundaries $r = 0$ and $r = \infty$ the pressure and its derivatives are

$$\begin{aligned} \hat{p}_0 &= C_1 I_m & \hat{p}_\infty &= C_2 K_m \\ \frac{d\hat{p}}{dr}_0 &= C_1 I'_m & \frac{d\hat{p}}{dr}_\infty &= C_2 K'_m \end{aligned} \quad (4.7)$$

Substituting the boundary values to the equation (4.6) and neglecting constant terms, the boundary conditions have the form

$$\chi_0 = -\alpha^2(U - c)\frac{I_m}{I'_m} \quad \chi_\infty = -\alpha^2(U - c)\frac{K_m}{K'_m} \quad (4.8)$$

For a value of ω , a guessed value of α is chosen, then Eq. (4.5) is integrated by means of the sixth order Runge-Kutta scheme from both sides χ_0 , the axis, and χ_∞ , a point sufficiently far from the axis. The two solutions are compared at $r = 1$ and if the curves do not meet, a new value of α is calculated according to the Newton-Ralphson method

$$\alpha^* = \alpha - J^{-1}(\chi_L - \chi_R) \quad (4.9)$$

Value α^* is only an estimation of the proper value for ω , so the procedure must be repeated until both sides appear with the same left (χ_L) and right (χ_R) value at $r = 1$, including a small error of the order of 10^{-5} . The J in Eq. (4.9) is the difference

$$J = \frac{d\chi_L}{d\alpha} - \frac{d\chi_R}{d\alpha} \quad (4.10)$$

Finally, ω or c is an eigenvalue and the continuous curve $\chi(r)$ is an eigenfunction of Equation (4.5). The above procedure is performed for complex ω in a wide range in order to obtain a $\alpha(\omega)$ map in the α complex space. Figure 2 presents the map for configuration with the back-flow (-0.3) and co-flow (0.3).

The pressure distribution \hat{p} can be easily obtained from χ using the relation

$$\hat{p}(r) = \hat{p}(r^*) \exp\left(-\int_{r^*}^r \frac{\alpha^2(U - c)}{\chi(r)} dr\right) \quad (4.11)$$

$\hat{p}(r^*)$ is a boundary value at a certain position $r = r^*$ and is unknown. Because of that, the pressure is normalized to obtain $\hat{p}_{max} = 1$. The authors have integrated the integral of Eq. (4.11) from the right side ($r^* = r_\infty$) towards zero, which seems to be more accurate.

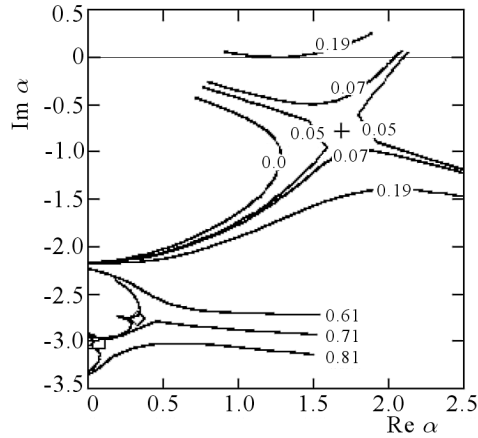


Fig. 2. Map of $\alpha(\omega)$ for configuration with back-flow (-0.3) and co-flow (0.3); a line is the image of α function for constant $\text{Im}(\omega)$, values denoted near the line

5. Results

5.1. Localization of absolutely unstable modes

The experiment revealed numerous saddle points for the considered configurations. Nevertheless, only one for each case satisfied the pinching requirement. The remaining points have been eliminated because they were located in a region above $\text{Im}(\omega(\alpha_m))$ of Eq. (2.6) or ω_i was negative. For example, in the double jet with recirculation zone (-0.3) and inflow (0.3), three saddle points were found with: (+) $\omega = 0.5014 + 0.0510i$, (\diamond) $\omega = 1.2742 + 0.7146i$ and (\square) $\omega = 1.4514 + 0.7323i$. The map $\alpha(\omega)$ of the configuration, Fig. 2, shows that the line of constant $\omega_i = 0.19$ has the highest ω imaginary part among the lines crossing the real α axis. This means that perturbation with the $\omega_i = 0.19$ is the wave most amplified in time. Accordingly, only the first saddle point is absolutely unstable.

As it was noted, no influence of the external co-flow on the stability (in fact on the locus of the single saddle point) was observed. Figure 3 presents the amplification rate ω_i as a function of the co-flow velocity.

Similarly, no change of the saddle point was observed in the presence of back-flow, neither in α nor in ω complex spaces. In the result, all configurations have the same absolutely unstable complex frequency $\omega = 0.501 + 0.051i$ and complex wave number $\alpha = 1.696 - 0.782i$.

5.2. Pressure distribution of the absolutely unstable mode

Surprisingly, the external flow with and without recirculation zone did not change the shape of the amplitude pressure disturbance. The pressure ampli-

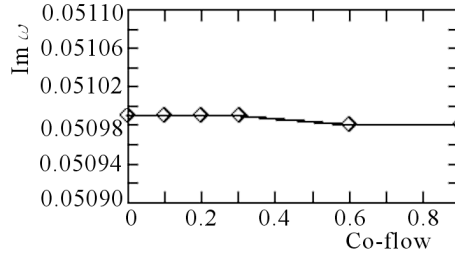


Fig. 3. Amplification rate ω_i as a function of co-flow velocity

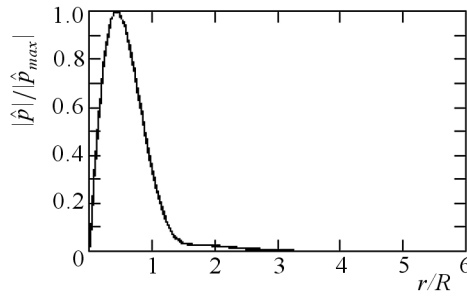


Fig. 4. Pressure distribution along the radial direction. The shape is the same for all configurations

tude, shown in Figure 4, is confined to the region of the first ring jet. It is zero on the axis and does not act on the secondary jet. The peak value of the eigenfunction is located in the vicinity of the first inflection point.

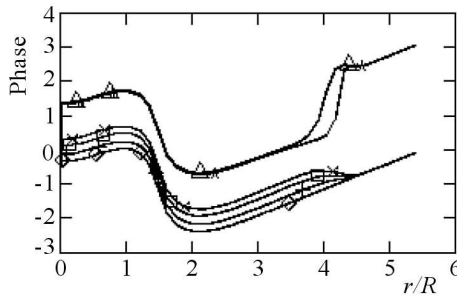


Fig. 5. Imaginary part of the pressure amplitude for flows without back-flow and with co-flow 0.0 (\diamond), 0.1 (+), 0.2 (\square), 0.3 (\times), 0.6 (\triangle), 0.9 (\star)

The presence of the additional flow is manifested only in the perturbation phase. For the configuration without the back-flow the phase is increasing with external stream, which is shown in Figure 5. The creation of recirculation zone has a similar effect. The phase shift is in the negative direction with the

increase of back-flow – Figure 6. However, the phase variation does not have any significant effect on physical behavior of the flow.

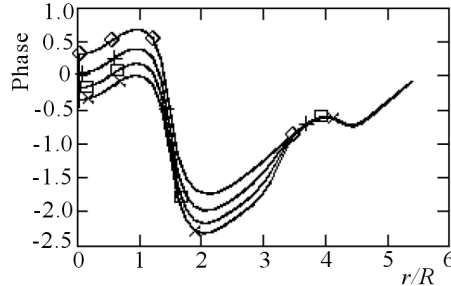


Fig. 6. Influence of the recirculation zone on the pressure amplitude phase. The co-flow is 0.3 and back-flow 0.0 (\diamond), -0.1 (+), -0.2 (\square), -0.3 (\times)

6. Summary

The linear spatio-temporal stability analysis allowed to identify complex parameters (α, ω) of the absolutely unstable modes in the presence of outer flow. Among many saddle points only one for each of the corresponding configurations was proved to be absolutely unstable. No influence of the external flow on the growth rate and wave length of the absolutely unstable mode was observed. Analysis of eigenfunctions showed also no significant change. Only a phase variation was noted, but it had no major physical consequences. The investigation was focused on asymmetric mode ($m = 1$) without swirl. Recent measurements of double ring jets Frania (2006), Frania and Hirsch (2005) showed that a flow without inlet swirl had a nonzero annular velocity close to the nozzle. It permits to expect additional unstable modes with the presence of a swirl. However, it is only an assumption of authors of the text based on the mean velocity data. In future the work will be extended to the analysis of double annular jet with inner and outer swirl.

Acknowledgment

The authors would like to acknowledge the State Committee for Scientific Research for financial support. The work was financed from the Statutory Research (BS) funds.

References

1. BERS A., 1983, Space-time evolution of plasma instabilities – absolute and convective, *Handbook of Plasma Physics*, **1**, 451-517, Amsterdam, North-Holland

2. BOGUSŁAWSKI A., 2002, *Niestabilność absolutna i konwekcyjna swobodnej osiowo-symetrycznej strugi płynu o niejednorodnej gęstości*, Monografia nr 85, Politechnika Częstochowska
3. BRIGGS R.J., 1964, *Electron-Stream Interaction With Plasmas*, Cambridge, Mass: MIT Press
4. CHOMAZ J.M., HUERRE P., REDEKOPP L.G., 1988, Bifurcations to local and global modes in spatially-developing flows, *Phys. Rev. Lett.*, **60**, 25
5. FAINBERG YA., KURILKO B., SHAPIRO V., 1961, Instabilities in the interaction of charged particle beams with plasmas, *Sov. Phys. Tech. Phys.*, **6**,
6. FRANIA T., 2006, *Experimental and Numerical Analysis of Annular Jet Flows*, PhD. Thesis, Vrije Universiteit Brussel
7. FRANIA T., HIRSCH CH., 2005, Measurement of the 3D turbulent flow field of confined double annular jet, *Abstract submitted for the 4th AIAA Theoretical Fluid Mechanics Conference*, Toronto
8. HUERRE P., MONKEWITZ P.A., 1990, Local and global instabilities in spatially developing flows, *Ann. Rev. Fluid Mech.*, **22**, 473-537
9. JENDOUBI J., STRYKOWSKI P.J., 1994, Absolute and convective instability of axisymmetric jets with external flow, *Phys. Fluids*, **6**, 9
10. MICHALKE A., 1999, Absolute inviscid instability of a ring jet with back flow and swirl, *Eur. J. Mech. B/Fluids*, **18**
11. MICHALKE A., HERMANN G., 1982, On the inviscid instability of a circular jet with external flow, *J. Fluid Mech.*, **114**, 343

Niestabilność absolutna podwójnej strugi pierścieniowej – analiza numeryczna

Streszczenie

W pracy analizuje się wpływ zewnętrznego przepływu na mody niestabilności absolutnej strugi pierścieniowej ze strefą recyrkulacji oraz podwójnej strugi pierścieniowej. Badania przeprowadzono przy użyciu liniowej, czasowo-przestrzennej teorii stabilności dla przepływów nielepkich. Do rozwiązania zagadnienia brzegowego wykorzystano metody numeryczne bazujące na algorytmie strzałów. W pracy uwzględniono tylko asymetryczne obwodowe mody niestabilności.

W trakcie eksperymentu numerycznego zidentyfikowano mody niestabilności absolutnej, nie stwierdzając wpływu zewnętrznego przepływu formującego zarówno strefę recyrkulacji, jak i drugą strugę pierścieniową, na stabilność przepływu.